Available online at www.sciencedirect.com
ScienceDirect
International Journal of Heat and Mass Transfer 50 (2007) 127–138
International Journal of HEAT and MASS TRANSFER
www.elsevier.com/locate/ijhmt

Numerical study of single bubbles with dynamic contact angle during nucleate pool boiling

Abhijit Mukherjee *, Satish G. Kandlikar

Mechanical Engineering Department, Rochester Institute of Technology, 76 Lomb Memorial Drive, Rochester, NY 14623, United States

Received 2 October 2005; received in revised form 27 June 2006
Available online 12 September 2006

Abstract

Nucleate pool boiling is typically characterized by cyclic growth and departure of vapor bubbles from a heated wall. It has been experimentally observed that the contact angle at the bubble base varies during the ebullition cycle. In the present numerical study, a static contact angle model and dynamic contact angle models based on the contact line velocity and the sign of the contact line velocity have been used at the base of a vapor bubble growing on a heated wall. The complete Navier–Stokes equations are solved and the liquid–vapor interface is captured using the level-set technique. The effect of dynamic contact angle on bubble dynamics and vapor volume growth rate is compared with results obtained with the static contact angle model.

Keywords: Bubble; Contact angle; Boiling

1. Introduction

Bubbles nucleate from cavities at the wall during nucleate pool boiling. During their growth period, the bubbles stay attached to the wall at the base. The bubble base diameter increases initially, then stays constant for a period of time and finally decreases as the bubble begins to depart. Intense evaporation is believed to take place near the bubble base that results in very high wall heat flux.

The contact angle made by the liquid–vapor interface at the bubble base with the wall varies during bubble growth and departure stages. This dynamic contact angle is different from static or equilibrium contact angle, which depends on the liquid and vapor properties and the material of the solid surface. The static contact angle does not have a unique value, as even under equilibrium conditions, the static advancing contact angle is different (larger) from the static receding contact angle.

Fig. 1 shows a nucleating bubble at the wall during nucleate pool boiling [1]. The frame on the left shows a bubble growing after its nucleation on the heater surface. The bubble base is expanding in this case, and the contact angle at the wall is receding. The frame on the right shows the same bubble just prior to departure. The bubble base is contracting in this case and the contact angle is advancing. It can be seen from these frames that the advancing contact angle is larger than the receding one.

The surface tension force acting at the bubble base depends on the dynamic contact angle. This affects the overall bubble dynamics and the wall heat transfer. The present numerical calculations are performed to study the effect of the dynamic contact angle at the bubble base as compared to a static contact angle.

2. Literature review

Researchers have extensively studied contact angle hysteresis for various solid–liquid combinations and surface conditions. Schulze et al. [2] empirically determined the equilibrium contact angle for certain low energy solids and pure liquids. They varied the roughness of the polymer

* Corresponding author. Tel.: +1 906 487 1174; fax: +1 906 487 2822.
E-mail addresses: mukherje@mtu.edu (A. Mukherjee), sgkeme@rit.edu (S.G. Kandlikar).

0017-9310/$ - see front matter © 2006 Elsevier Ltd. All rights reserved.
doi:10.1016/j.ijheatmasstransfer.2006.06.037

Nomenclature

ACA	advancing contact angle
C_p	specific heat at constant pressure
d	grid spacing
g	gravity vector
H	Heaviside function
h_{fg}	latent heat of evaporation
k	thermal conductivity
l_0	length scale
m	mass transfer rate at interface
ms	milliseconds
p	pressure
r	bubble base radius
RCA	receding contact angle
Re	Reynolds number
T	temperature
ΔT	temperature difference, $T_w - T_{sat}$
t	time
u	x direction velocity
u_0	velocity scale
V	contact line velocity at bubble base
v	y direction velocity
w	z direction velocity
x	distance in x direction
y	distance in y direction
z	distance in z direction

Greek symbols

α	thermal diffusivity
β_T	coefficient of thermal expansion
κ	interfacial curvature
μ	dynamic viscosity
ν	kinematic viscosity
ρ	density
σ	surface tension
τ	time period
ϕ	level set function
φ	contact angle

Subscripts

a	advancing
evp	evaporation
l	liquid
lim	limiting
r	receding
sat	saturation
v	vapor
w	wall
x	$\partial/\partial x$
y	$\partial/\partial y$
z	$\partial/\partial z$

Superscripts

*	non-dimensional quantity
$\rightarrow$	vector quantity

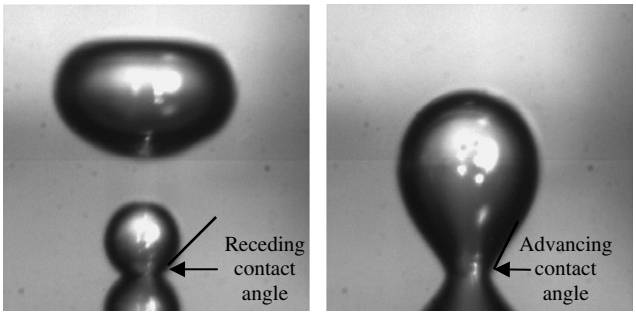

Fig. 1. Dynamic contact angle at bubble base during nucleate pool boiling [1].

solid surfaces and used a sessile drop experiment to measure the advancing and receding contact angles. The contact angle hysteresis was assumed to be dependent on the surface roughness and the equilibrium contact angle was linearly approximated setting the hysteresis to be zero. Shoji and Zhang [3] experimentally measured contact angle of water on copper, glass, aluminum and Teflon surfaces. The receding contact angle was found to decrease with surface roughness while the advancing contact angle remained almost constant. They also developed a model for evaluating surface wettability by introducing a surface roughness parameter and a surface energy parameter. They concluded that the advancing and receding contact angles are unique for any liquid–solid combination and the surface condition.

Brandon and Marmur [4] simulated contact angle hysteresis for a two-dimensional drop on a chemically heterogeneous surface. The intrinsic contact angle was assumed to vary periodically with distance from the center of the drop. The changes in free energy of the system, the contact angle and the size of the base of the drop were calculated with changes in the volume of the drop. The authors concluded that the quasi-static analysis of the dependence of the free energy of the system on the drop volume could explain the contact angle hysteresis measurements. Kandlikar and Steinke [5] made photographic observations of liquid droplets impinging on a heated surface. They studied the effects of surface roughness and surface temperatures on the dynamic advancing and receding contact angles. They found that the equilibrium contact angle first decreased and then increased with surface roughness. The dynamic advancing and receding contact angles were found to be equal for high wall superheats at critical heat flux

conditions. Lam et al. [6] carried out dynamic one-cycle and cyclic contact angle measurements for different solids and liquids. Four different patterns of receding contact angle were obtained: (a) time dependent receding contact angle; (b) constant receding contact angle; (c) stick/slip pattern and (d) no receding contact angle. The authors identified liquid sorption and retention as the primary cause of contact angle hysteresis.

Apart from the physical properties and surface conditions of the solid–liquid combination, the contact angle hysteresis is also believed to be influenced by the liquid–vapor interface velocity. Ramanujapu and Dhir [7] studied dynamic contact angle at the base of a vapor bubble during nucleate pool boiling. A silicon wafer was used as the test surface with micromachined cavities for nucleation. The bubble base diameter was measured as a function of time and the interface velocity was calculated. The results show that though the contact angle varied during different stages of bubble growth, it was weakly dependent on the interface velocity. They concluded that contact angle could be determined primarily based on the sign of the interface velocity.

Sobolev et al. [8] measured dynamic contact angle of water in thin quartz capillaries with radii varying from 200 to 40 nm. The value of dynamic contact angle was found to depend on the degree of surface coverage by the absorbed water molecules. At velocities less than 5 μm/s, the dynamic contact angle was found to be linearly dependent on the velocity whereas, at higher velocities, it was found to be rate independent. Barraza et al. [9] determined advancing contact angle during spontaneous capillary penetration of liquid between two parallel glass plates by measuring the transient height attained by it. The data was fitted into an averaged Navier–Stokes model integrated over a cross section away from the liquid front. The calculated contact angle values failed to predict the dependence of the dynamic contact angle on velocity as suggested by classical hydrodynamics and molecular theories in the non-wetting case. Kandlikar et al. [10] experimentally studied an evaporating meniscus on a smooth heated rotating copper surface. They studied the size and shape of the meniscus and the receding and advancing contact angles for various surface velocities and wall superheat. Large difference was observed between the advancing and receding contact angles. At wall superheat of 102.5 °C, the advancing and receding contact angles were found to be almost constant for various surface velocities, but at 105.5 °C the receding contact angle decreased at higher velocities. At 108 °C wall superheat, both advancing and receding contact angles started to fluctuate with increase in surface velocity, due interface instabilities caused by high evaporation rate.

Several studies have appeared in the literature on the effect of contact angle on bubble growth during nucleate boiling. Kandlikar and Stumm [11] developed a model to analyze the forces acting on a vapor bubble during subcooled flow boiling. They also measured experimentally the upstream and downstream contact angles as a function of flow velocity. They found that the departing bubble size became smaller and the upstream and downstream contact angles went through a maxima and minima, respectively, with increase in flow velocity. Son et al. [12] carried out complete numerical simulation of a single bubble on a horizontal surface during nucleate pool boiling. They assumed a static contact angle at the bubble base and accounted for the microlayer evaporation by including the disjoining pressure effect. The results showed that the departing bubble became larger with increase in contact angle. Kandlikar [13] developed a theoretical model of CHF with dynamic receding contact angle. The model was based on the assumption that CHF occurs when the force due to the momentum change pulling the bubble interface into the liquid along the heated surface exceeds the sum of the forces from surface tension and gravity holding the bubble. He assumed the dynamic receding contact angle for various liquid–solid systems. The model indicated decrease in CHF with increase in contact angle. Abarajith and Dhir [14] numerically studied the effect of contact angle on single bubbles during nucleate pool boiling. The contact angle was kept fixed throughout the bubble growth and departure process. The effect of microlayer evaporation was included in the study. The contact angle was related to the magnitude of the Hamaker constant, which was found to change with surface wettability. The bubble departure diameter and time was found to increase with increase in contact angle.

Researchers have incorporated different models of dynamic contact angle during numerical simulations of droplet motion. Fukai et al. [15] theoretically and experimentally studied deformation of a liquid droplet colliding and spreading on a flat surface. The wetting effect was accounted for using constant distinct values of advancing and receding contact angles during spreading and recoiling process. The values of the constant dynamic contact angle used in the mathematical model were obtained experimentally from a droplet sliding freely down an inclined test surface. This was done in spite of the fact that velocity magnitude of sliding droplet was smaller than impacting droplet and dynamic contact angle is known to be dependent on the velocity. The numerically obtained droplet shapes qualitatively agreed with experimental data.

Bussman et al. [16] developed a three-dimensional numerical model of droplet impact onto asymmetric surfaces. Two cases were studied; impact of a droplet on an incline and onto a sharp edge. The fixed grid Eulerian model employed first-order accurate Young's volume tracking algorithm to track droplet free surface. Two methods were used to specify the contact angle boundary condition. In the first method, the advancing and receding contact angle obtained from experiments was specified only if the corresponding contact line velocity was greater than 0.1 m/s. At contact line locations with velocity less than 0.1 m/s, the contact angle was specified using linear interpolation between the nearest known values at the leading and trailing edges. In the second method, the contact angle

was specified as a linear function of contact line velocity between 0.1 m/s and 0.05 m/s. Above 0.1 m/s constant values of advancing and receding contact angle was specified as appropriate whereas below 0.05 m/s a constant equilibrium value of contact angle was assumed. Both methods produced similar results except for some difference in the equilibrium droplet shapes.

Son and Hur [17] simulated droplet motion on an inclined wall using level-set method on non-orthogonal grids. They implemented two different contact angle formulations at the gas–liquid–solid interline. In the first formulation same value of advancing and receding contact angle was used. In the second formulation different but constant values of advancing and receding contact angle was specified. Under conditions of no gravity the shapes attained by the droplets using both the contact angle formulations matched well with the exact solutions. However, no validation of the above formulations was presented under dynamic conditions of droplet motion.

3. Numerical model

3.1. Method

The present study uses the numerical model of Mukherjee and Dhir [18] to simulate vapor bubble growth on a heated wall. The numerical analysis is done by solving the complete incompressible Navier–Stokes equations using the SIMPLE method [19], which stands for semi-implicit method for pressure-linked equations. A pressure field is extracted from the given velocity field. The continuity equation is turned into an equation for the pressure correction. During each iteration, the velocities are corrected using velocity-correction formulas. The "consistent" approximation [20] is used for the velocity correction. The resulting velocity field exactly satisfies the discretized continuity equation, irrespective of the fact that the underlying pressure corrections are only approximate. The computations proceed to convergence via a series of continuity satisfying velocity fields. The algebraic equations are solved using the line-by-line technique, which uses TDMA (tri-diagonal matrix algorithm) as the basic unit. The speed of convergence of the line-by-line technique is further increased by supplementing it with the block-correction procedure [21]. Multi-grid technique is used to solve the pressure fields.

Sussman et al. [22] developed a level set approach where the interface was captured implicitly as the zero level set of a smooth distance function. The level set function was typically a smooth function, denoted as ϕ. This formulation eliminated the problems of adding/subtracting points to a moving grid and automatically took care of merging and breaking of the interface. The present analysis is done using this level set technique.

The liquid vapor interface is identified as the zero level set of a smooth distance function ϕ. The level set function ϕ is negative inside the bubble and positive outside the bubble. The interface is located by solving the level set equation. A fifth-order WENO (weighted, essentially non-oscillatory) scheme is used for left sided and right sided discretization of ϕ [23]. While ϕ is initially a distance function, it will not remain so after solving the level set equation. Maintaining ϕ as a distance function is essential for providing the interface with a width fixed in time. This is achieved by reinitialization of ϕ. A modification of Godunov's method is used to determine the upwind directions. The reinitialization equation is solved in fictitious time after each fully complete time step. With $\Delta\tau = \frac{d}{2u_0}$, ten τ steps are taken with a third-order TVD (total variation diminishing) Runge Kutta method.

3.2. Governing equations

Momentum equation

$$\rho\left(\frac{\partial \vec{u}}{\partial t} + \vec{u}\cdot\nabla\vec{u}\right) = -\nabla p + \rho\vec{g} - \rho\beta_{\mathrm{T}}(T - T_{\mathrm{sat}})\vec{g} - \sigma\kappa\nabla H + \nabla.\mu\nabla\vec{u} + \nabla.\mu\nabla\vec{u}^{\mathrm{T}} \tag{1}$$

Energy equation

$$\rho C_p\left(\frac{\partial T}{\partial t} + \vec{u}\cdot\nabla T\right) = \nabla\cdot k\nabla T \quad \text{for } \phi > 0$$
$$T = T_{\mathrm{sat}} \quad \text{for } \phi \leqslant 0 \tag{2}$$

Continuity equation

$$\nabla\cdot\vec{u} = \frac{\vec{m}}{\rho^2}\cdot\nabla\rho \tag{3}$$

The curvature of the interface is defined as

$$\kappa(\phi) = \nabla\cdot\left(\frac{\nabla\phi}{|\nabla\phi|}\right) \tag{4}$$

The mass transfer rate of liquid evaporating at the interface

$$\vec{m} = \frac{k_{\mathrm{l}}\nabla T}{h_{\mathrm{fg}}} \tag{5}$$

The vapor velocity at the interface due to evaporation

$$\vec{u}_{\mathrm{evp}} = \frac{\vec{m}}{\rho_{\mathrm{v}}} = \frac{k_{\mathrm{l}}\nabla T}{\rho_{\mathrm{v}}h_{\mathrm{fg}}} \tag{6}$$

To prevent instabilities at the interface, the density and viscosity are defined as

$$\rho = \rho_{\mathrm{v}} + (\rho_{\mathrm{l}} - \rho_{\mathrm{v}})H \tag{7}$$
$$\mu = \mu_{\mathrm{v}} + (\mu_{\mathrm{l}} - \mu_{\mathrm{v}})H \tag{8}$$

H is the Heaviside function

$$H = 1 \quad \text{if } \phi \geqslant +1.5d$$
$$H = 0 \quad \text{if } \phi \leqslant -1.5d$$
$$H = 0.5 + \phi/(3d) + \sin[2\pi\phi/(3d)]/(2\pi) \quad \text{if } |\phi| \leqslant 1.5d \tag{9}$$

where d is the grid spacing.

Since the vapor is assumed to remain at saturation temperature, the thermal conductivity is given by

$$k = k_l H^{-1} \tag{10}$$

Level set equation is solved as

$$\frac{\partial \phi}{\partial t} + (\vec{u} + \vec{u}_{evp}) \cdot \nabla \phi = 0 \tag{11}$$

After every time step, the level-set function ϕ is reinitialized as

$$\frac{\partial \phi}{\partial t} = S(\phi_0)(1 - |\nabla \phi|)u_0 \qquad \phi(x,0) = \phi_0(x) \tag{12}$$

S is the sign function which is calculated as

$$S(\phi_0) = \frac{\phi_0}{\sqrt{\phi_0^2 + d^2}} \tag{13}$$

3.3. Computational domain

Fig. 2 shows the computational domain which is $0.99 \times 1.98 \times 0.99$ non-dimensional units in size. Cartesian coordinates are used with uniform grid. The bottom of the domain is defined as the wall. The bubble is placed at the wall. Taking advantage of symmetry, calculations are done for one quarter of the bubble. The number of computational cells in the domain are $72 \times 144 \times 72$ i.e. 72 grids are used per $0.99 l_0$. These values are the same as used by Mukherjee and Dhir [18] to optimize numerical accuracy and computation time. Experimental validation of the present numerical code has been provided earlier by Mukherjee and Dhir [18].

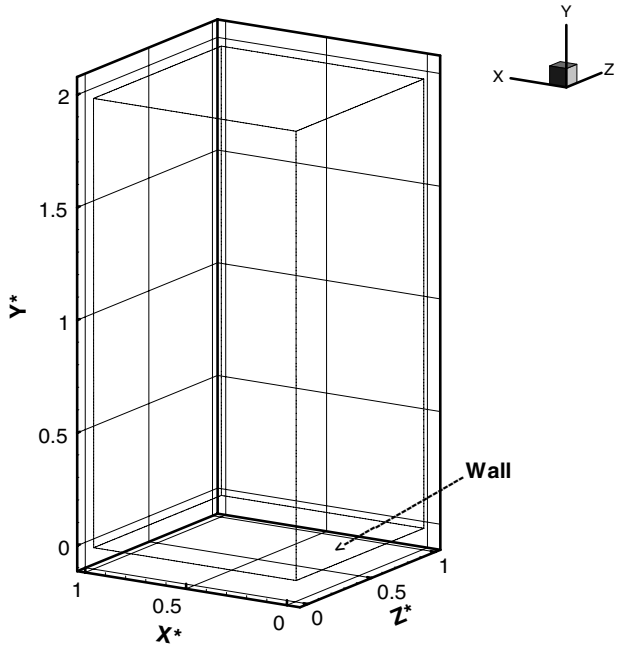

Fig. 2. Computational domain.

3.4. Scaling factors

The governing equations are made non-dimensional using a length scale (l_0) and a time scale (t_0) defined by,

$$l_0 = \sqrt{\frac{\sigma}{g(\rho_l - \rho_v)}} \tag{14}$$

$$t_0 = \sqrt{\frac{l_0}{g}} \tag{15}$$

The characteristic velocity is thus given by,

$$u_0 = \frac{l_0}{t_0} \tag{16}$$

The non-dimensional temperature is defined as,

$$T^* = \frac{T - T_{sat}}{T_w - T_{sat}} \tag{17}$$

with $T^* = 0$ when $T = T_{sat}$ and $T^* = 1$ at the wall when $T = T_w$.

3.5. Initial conditions

A spherical bubble of radius 0.1 non-dimensional length is placed in the domain on the wall, with the given contact angle. The initial coordinates for the center of a single bubble would be $(0, r\cos\varphi, 0)$. All initial velocities are set to zero. The initial thermal boundary layer thickness is calculated from the correlation for the turbulent natural convection heat transfer. The initial thickness is given by

$$\delta_t = 7.14(\nu_l \alpha_l / g\beta_T \Delta T)^{1/3} \tag{18}$$

The liquid and vapor properties are taken for water at 100 °C. The vapor temperature is set to the saturation temperature i.e. 100 °C. The wall temperature is set to 110 °C for all cases and this corresponds to the partial nucleate boiling regime.

3.6. Boundary conditions

The boundary conditions are as follows:

At the wall ($y^* = 0$):

$$u^* = v^* = w^* = 0; \quad T^* = 1, \quad \frac{d\phi}{dy} = -\cos\varphi \tag{19}$$

where φ is the contact angle.

At the planes of symmetry ($x^* = 0$, $x^* = 1$):

$$u^* = v_x^* = w_x^* = T_x^* = 0 \tag{20}$$

At the planes of symmetry ($z^* = 0$, $z^* = 1$):

$$u_z^* = v_z^* = w^* = T_z^* = 0 \tag{21}$$

At the top of the domain ($y^* = 2$):

$$u_y^* = v_y^* = w_y^* = 0, \quad T^* = 0 \tag{22}$$

3.7. Microlayer evaporation

Several previous studies [1,12,14,18] of single vapor bubbles growing on a heated wall have included the effect of microlayer evaporation. Son et al. [12] reported microlayer contribution to be about 20% for a certain set of calculations. The transient conduction due to liquid motion being major contributor to wall heat transfer in nucleate boiling, the effect of contact angle on bubble dynamics is the focus of this work. Since the effect of microlayer is seen to be small and no reliable experimental data on microlayer thickness under the bubble is available, the present simulation is carried out to highlight the effect of liquid motion and transient conduction around a bubble. Hence the effect of microlayer evaporation at the bubble base has been excluded in the subsequent calculations.

4. Results

Five different cases have been studied:

Case 1: Static contact angle of 54°.
Case 2: Constant advancing contact angle of 61° and constant receding contact angle of 48°.
Case 3: Advancing and receding contact angle as function of contact line velocity.
Case 4: Constant advancing contact angle of 90° and constant receding contact angle of 54°.
Case 5: Constant advancing contact angle of 54° and constant receding contact angle of 20°.

In Cases 4 and 5 one of the dynamic contact angles is 54° which is same as the static contact angle used in Case 1. The 90° advancing contact angle is chosen in Case 4 to represent surfaces with low wettability. The 20° receding contact angle is chosen in Case 5 to represent surfaces with high wettability with same amount of hysteresis as in Case 4.

Fig. 3 shows the experimental data obtained by Ramanujapu and Dhir [7] for variation of contact angle at the base of a single vapor bubble. They plotted the contact angle as a function of interface velocity. The plot shows an approximate maximum advancing contact angle of 61° and an approximate minimum receding contact angle of 48°. The fitted curve shows a linear variation of contact angle between limiting interface velocities. The static contact angle was 54° for the test surface. The data from Fig. 3 has been used in Cases 1–3.

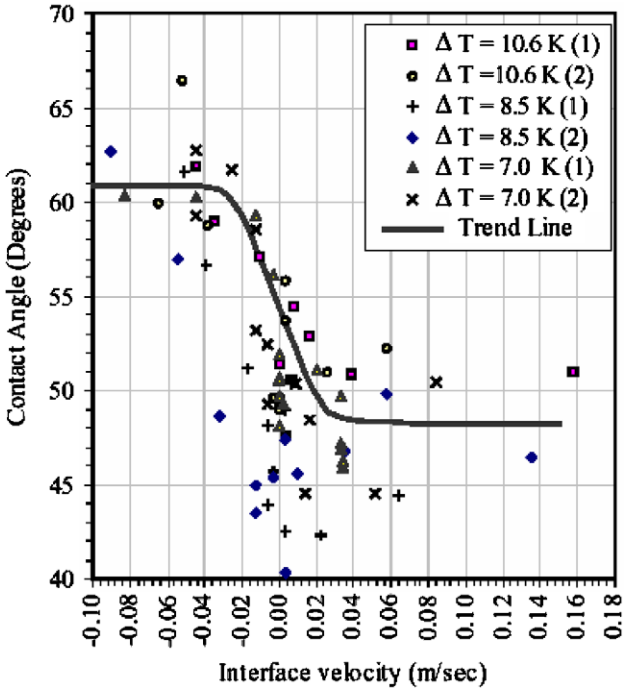

Fig. 3. Experimental observation of dynamic contact angle at bubble base during nucleate pool boiling [7].

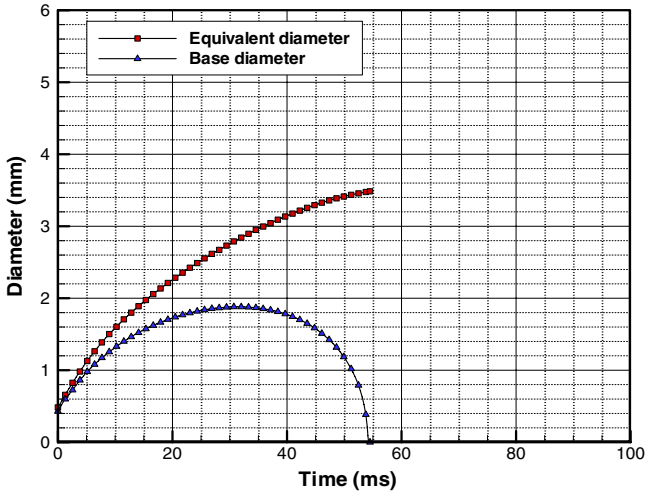

Fig. 4. Bubble growth, static contact angle 54°.

4.1. Case 1 – static contact angle

Numerical simulation of a single bubble has been carried out with a static contact angle of 54°. Fig. 4 plots the equivalent bubble diameter and the bubble base diameter as a function of time. The bubble equivalent diameter is calculated assuming a sphere of equal volume. The bubble base diameter is found to increase initially and stay constant at 1.85 mm at around 30 ms. The base diameter decreases thereafter and becomes zero at 54 ms. This indicates bubble departure with an equivalent diameter of 3.5 mm.

4.2. Case 2 – constant advancing and receding contact angles

Fig. 5 shows the results of numerical calculations with different advancing and receding contact angles. In this

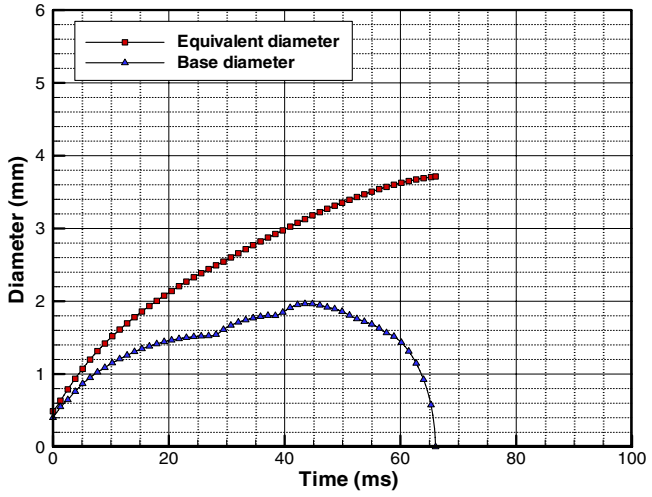

Fig. 5. Bubble growth, receding contact angle 48°, advancing contact angle 61°.

case, the contact angle is specified depending on the sign of the contact line velocity. Thus, when the bubble base diameter is increasing, the contact angle is specified as 48° whereas when the bubble base diameter is decreasing, the contact angle is specified as 61°. The rate of change in bubble base diameter is high initially but slows down around 28 ms. Thereafter, as the base diameter tries to decrease, the contact angle immediately changes to advancing contact angle and becomes higher. This affects the surface tension force at the bubble base. The increase in contact angle decreases the surface tension force that was causing the bubble base to contract. As a result, the bubble base starts to expand again after 28 ms at a higher rate. The contact angle at the bubble base keeps changing in the calculations depending on whether the base diameter is trying to increase or decrease. A sudden increase in the rate of change of the bubble base diameter is again observed at 40 ms. This phenomenon of sudden increase in the rate of change of bubble base diameter is caused due to specification of dynamic contact angle at the bubble base which is evident from comparing Cases 1 and 2.

The expansion/contraction of the bubble base depends on force balance parallel to the wall which includes surface tension, evaporation momentum, inertia and viscous forces. The surface tension force tries to contract the bubble base whereas the evaporation momentum force tries to expand it. When the contact angle increases due to a switch from receding to advancing, the surface tension force decreases, causing the evaporation momentum force to dominate. The inertia imparted to the bubble base due to this sudden force imbalance causes the bubble base to re-expand even though the contact angle switches back to a lower (receding) value. In Case 2, the bubble base 'sticks' around 27 ms and 38 ms with the contact line velocity reaching zero as seen in Fig. 5. Shortly thereafter, the bubble base 'slips' with the contact line accelerating and the bubble base tries to expand again.

Dussan [24] explains slip/stick behavior as when the motion of a contact line appears to be unsteady and spasmatic and it occurs below a certain smallest reported speed. Above that speed the contact line movement is found to be very smooth. The slip/stick behavior may occur in a cyclic pattern as observed by Lam et al. [6] while measuring dynamic contact angle of a sessile drop of *n*-pentadecane on FC-732-coated silicon wafer.

The overall bubble base diameter (Fig. 5) keeps increasing while exhibiting the stick/slip pattern till 44 ms, after which it decreases till bubble departure. The bubble departs at 66 ms with a higher equivalent bubble diameter compared to the previous case where a static contact angle was assumed.

Comparing Figs. 4 and 5, it can be seen that incorporating different (but constant) advancing and receding contact angles results in a stick/slip interface movement at the base during the bubble growth.

4.3. Case 3 – dynamic contact angle as a function of interface velocity

Numerical calculations are carried out with dynamic contact angle at the bubble base as obtained from Fig. 3. The contact angle is specified as follows:

$$\begin{aligned} \varphi &= \varphi_a \quad \text{for } \frac{dr}{dt} < -V_{lim} \\ \varphi &= \varphi_r \quad \text{for } \frac{dr}{dt} > V_{lim} \\ \varphi &= \frac{\varphi_r - \varphi_a}{2V_{lim}}\left(\frac{dr}{dt}\right) + \frac{\varphi_r + \varphi_a}{2} \quad \text{for } \left|\frac{dr}{dt}\right| \leqslant V_{lim} \end{aligned} \tag{23}$$

where $\frac{dr}{dt}$ is the rate of change of bubble base radius, V_{lim} is the limiting contact line velocity and $\varphi_r = 48°$ and $\varphi_a = 61°$. It may be noted here that in Fig. 3, the interface velocity is defined as the rate of change of bubble base diameter (and not radius) with time.

Fig. 6 shows plot of the bubble and base diameters against time for this case. Results of two calculations are presented with $V_{lim} = 0.02$ m/s and 0.04 m/s. In these cases, the base contact angle changes dynamically during the bubble growth between the specified limiting advancing and receding contact angles. For the case with $V_{lim} = 0.04$ m/s, the rate of change of base diameter does not show any overall fluctuations. In fact, the variation in the bubble base diameter is smooth and comparable to the results in Case 1 with a static contact angle of 54°. However, in the case of $V_{lim} = 0.02$ m/s, the changes in bubble base diameter is comparatively less smooth. Thus, as V_{lim} is decreased, the behavior of the bubble base approaches the stick/slip pattern observed in Case 2 and as V_{lim} is increased, the behavior of the bubble base approaches static constant angle pattern of Case 1. In both these cases with dynamic contact angle as a function of the contact line velocity, the bubble departure time is around 60 ms which is comparatively longer than that in Case 1 but less than Case 2.

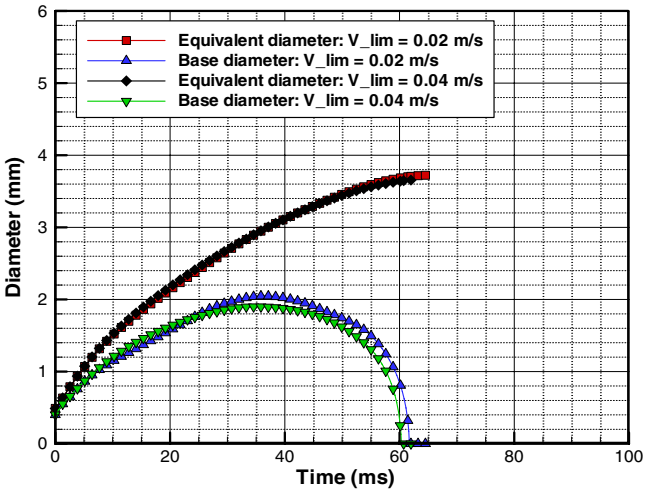

Fig. 6. Bubble growth, contact angle between 48° and 61°, as a function of contact line velocity.

4.4. Case 4 – constant advancing contact angle of 90° and receding contact angle of 54°

Calculations were performed for a case with constant advancing contact angle of 90° and constant receding contact angle of 54°, high values of contact angle indicating that the surface is non-wetting in nature. It has been previously demonstrated [12] that the bubble departure diameter increases with increase in contact angle. Thus, a bigger computation domain of size $1.43 \times 2.86 \times 1.43$ non-dimensional units is used for this case. Fig. 7 shows the bubble shapes obtained in Case 4. The time corresponding to the shapes is indicated on each frame. The bubble initially grows with a spherical shape but gradually turns into a hemispherical shape due to the effect of high advancing contact angle. When the bubble departs, the bubble base forms a neck which is seen in the frame corresponding to 85.5 ms.

Fig. 8 shows the bubble growth rate corresponding to Case 4. The bubble initially grows similar to Case 1 with constant receding angle of 54°. At around 32 ms, the rate of increase of bubble base diameter almost becomes zero and as the bubble base tries to contract the contact angle changes to 90°. The bubble base exhibits the stick/slip behavior and it tries to expand at a faster rate. At around 50 ms, the bubble diameter and base diameter becomes equal. Between 50 and 65 ms the base diameter remains almost constant while the bubble equivalent diameter increases. Thereafter, the bubble base shrinks continuously and bubble departs at around 88 ms with an equivalent departure diameter of 5.4 mm.

4.5. Case 5 – constant advancing contact angle of 54° and receding contact angle of 20°

Calculations were also performed for a case with constant advancing contact angle of 54° and constant receding

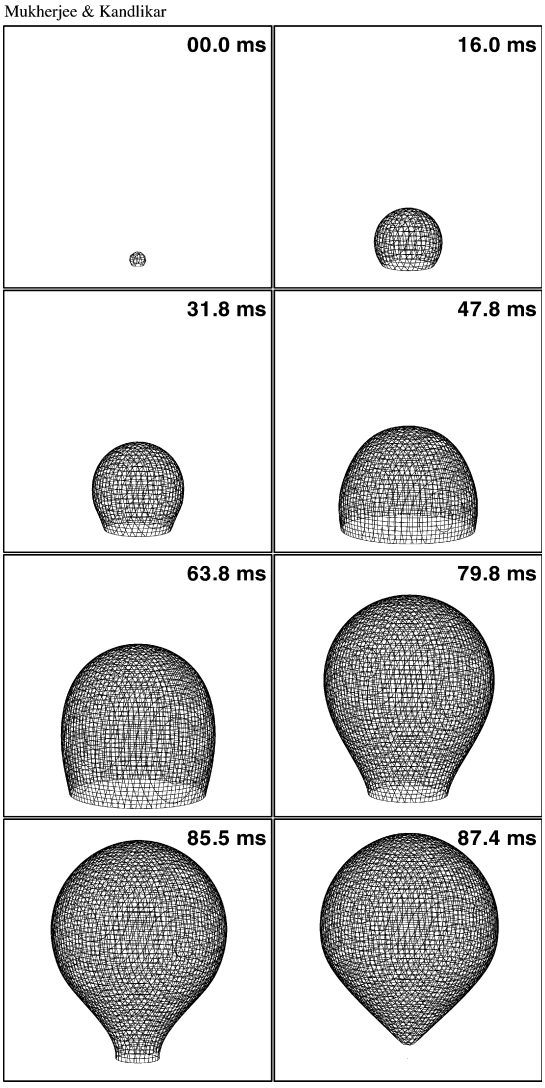

Fig. 7. Bubble shapes, receding contact angle 54°, advancing contact angle 90°.

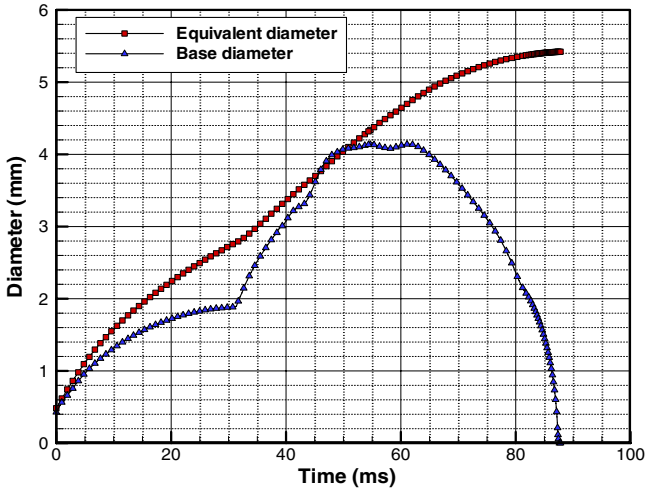

Fig. 8. Bubble growth, receding contact angle 54°, advancing contact angle 90°.

contact angle of 20°. Thus, in this case the amount of hysteresis is similar to Case 4, however with lower values of contact angles, i.e. the surface is wetting in nature. Fig. 9 shows the bubble shapes obtained in Case 5. The time corresponding to the shapes is indicated on each frame. The bubble grows with a spherical shape during the entire growth period. There is no neck formation at the bubble base when it departs at 42 ms.

Fig. 10 shows the bubble growth rate corresponding to Case 5. The stick/slip behavior of the bubble base is noted around 4 ms. The bubble base starts to contract continuously after 25 ms and the bubble departs at around 42 ms with an equivalent diameter of 3 mm. The stick/slip behavior of the bubble base in this case is limited to only the early stages of bubble growth whereas in Case 4, the bubble base exhibited the stick/slip behavior through a significant part of the bubble growth period. Thus, it can be concluded that stick/slip behavior of the bubble base due to contact angle hysteresis becomes more pronounced as the surface wettability decreases.

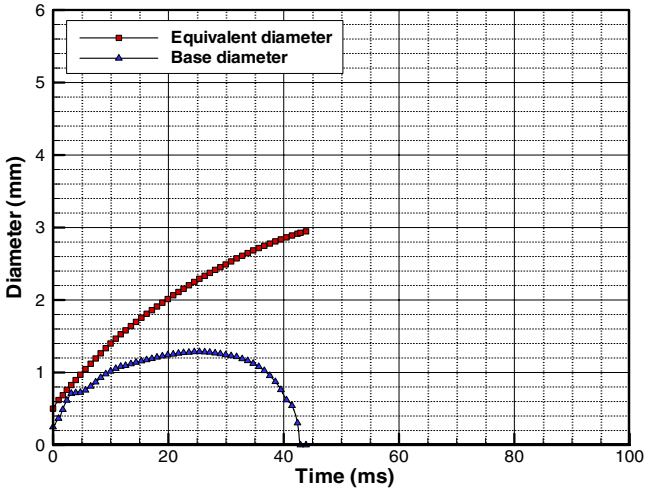

Fig. 10. Bubble growth, receding contact angle 20°, advancing contact angle 54°.

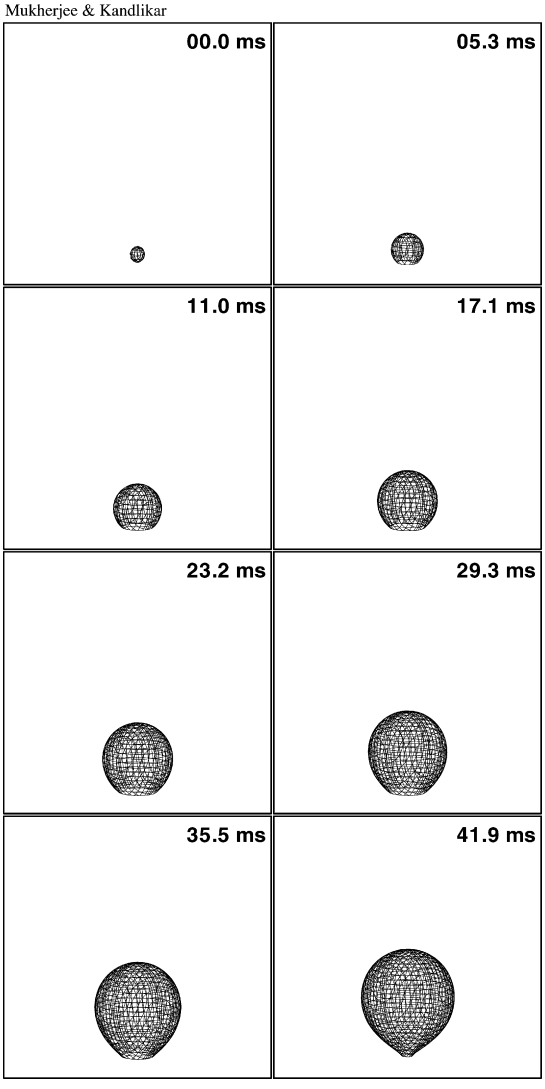

Fig. 9. Bubble shapes, receding contact angle 20°, advancing contact angle 54°.

5. Discussion

Fig. 11 compares the vapor volume growth rates for the five cases. The vapor volume growth rate is calculated by dividing the bubble departure volume with departure time. Case 3 represents the simulation of the actual experimental conditions shown in Fig. 3 with $V_{\text{lim}} = 0.04$ m/s.

It can be seen that for the first three cases, there is little difference between the vapor volume growth rates. Therefore the effect of contact angle hysteresis on the vapor removal rate is negligible for these three cases, with Cases 2 and 3 having the same limiting values of advancing and receding contact angles. In Case 4 with 90° advancing contact angle, the vapor generation rate is more than twice compared to the previous cases. However, in Case 5, which has the same amount of hysteresis as Case 4, but

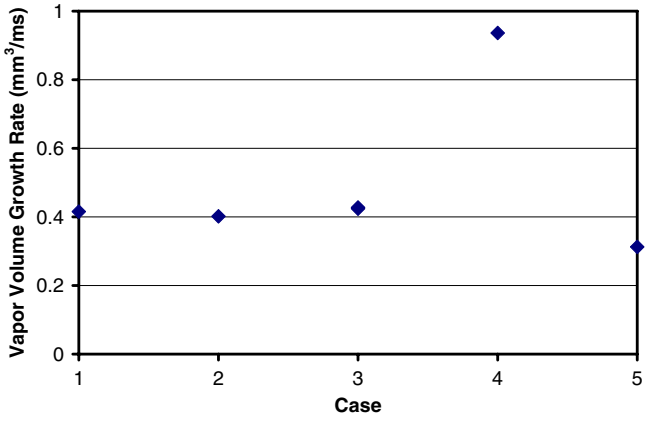

Fig. 11. Comparison of vapor volume growth rates (Case 3 with $V_{\text{lim}} = 0.04$ m/s).

20° receding contact angle, the vapor volume growth rate is only 25% lower as compared to the first three cases. Two primary conclusions can be drawn from comparing the vapor volume growth rates of Cases 2, 4 and 5. First, the vapor volume growth rate is primarily determined by the advancing contact angle as compared to the receding contact angle. Second, the vapor volume growth rate increases as the surface becomes less wetting. The second conclusion is consistent with the experimental findings of Liaw and Dhir [25]. They experimentally studied variation of wall heat flux for various contact angles at higher end of nucleate boiling. Their results showed that as the surface wettability improved i.e. as the contact angle decreased, a higher superheat was required to attain the same heat flux.

The vapor volume growth rate depends directly on the wall heat flux that supplies the latent heat for the phase change. The reasons for increase in wall heat flux with increase in contact angle can be determined by looking at the velocity and temperature fields around the bubble.

Fig. 12 compares the velocity fields near the bubble base, the bottom frame showing Case 4 and the top frame showing Case 5. The frames are chosen such that both the bubbles are in the departing stages with same bubble base diameters. The shrinking of bubble base creates a clockwise liquid circulation around it that draws cooler saturated liquid towards the wall. However, for the case with large contact angle this circulation is much more pronounced with larger velocity vectors and involving a larger amount of liquid. Thus, as the surface wettability decreases, the bubble attains a larger departure diameter and creates a bigger vortex around it when it departs.

Fig. 13 compares the temperature field around the vapor bubble base prior to departure for Cases 4 and 5. Isotherms (T^*) are plotted at intervals of 0.1. The bottom frame shows that the liquid circulation near the bubble base with the 90° advancing contact angle has effectively moved larger amount of superheated liquid away from the wall, as compared to case with 54° advancing contact angle in the top frame. Also, as the bubble lifts off, the clockwise vortex causes the saturated liquid to move down towards the wall at the edge of the computational domain, which pushes the thermal boundary layer against the wall. The thermal boundary layer at the edge of the computational domain is thinner in the bottom frame (at $x^* = 1.4$) due to the stronger vortex as compared to the top frame (at $x^* = 0.99$). Thus, the bigger vortex created during bubble departure on the less wetting surface is more effective in disturbing the thermal boundary layer around it, thereby increasing the overall wall heat transfer.

Summarizing the effect of different models of dynamic contact angle at the bubble base (Cases 1–3) it can be said

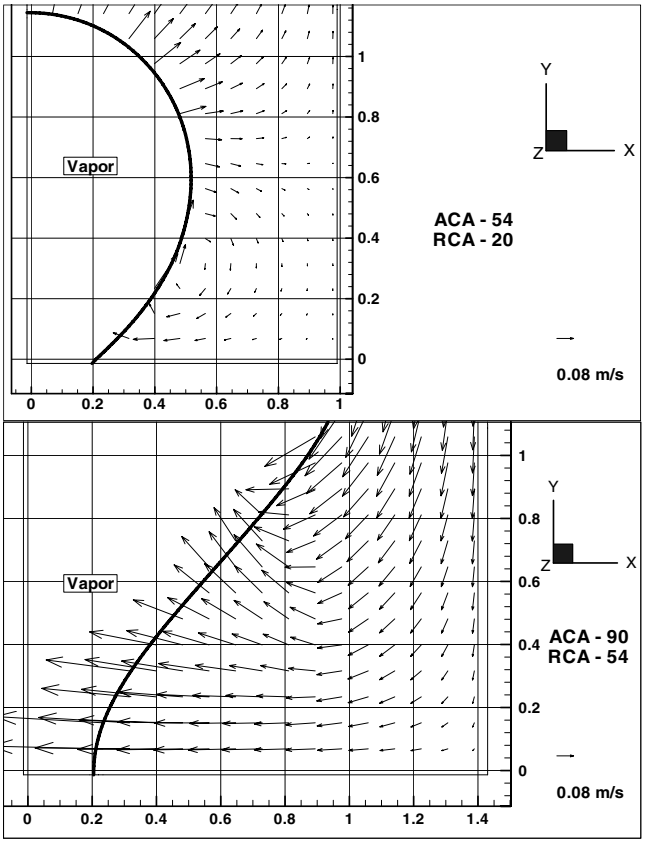

Fig. 12. Velocity field in liquid near the bubble base.

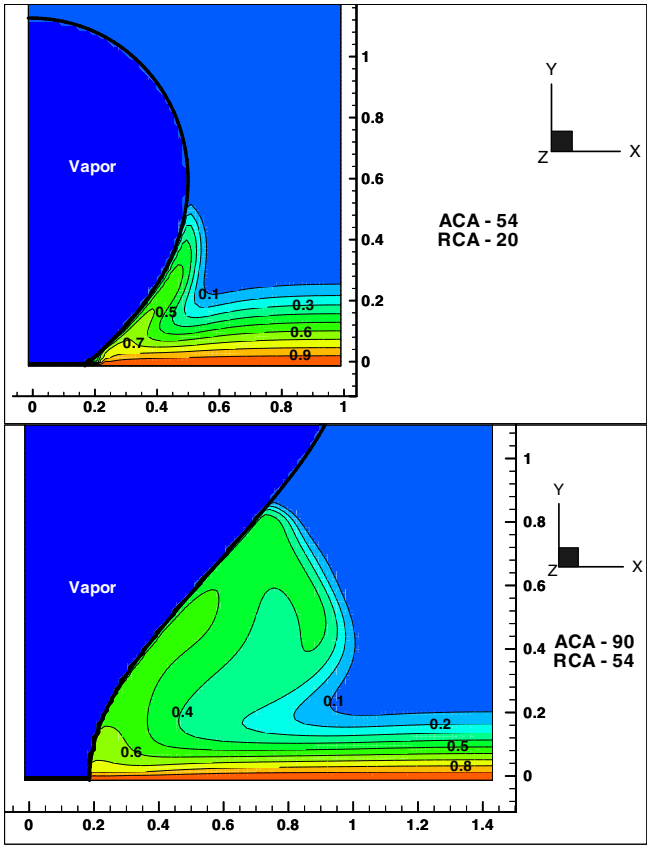

Fig. 13. Temperature field near the bubble base.

that bubble nucleation simulation is best done with dynamic contact angle as a function of interface velocity (Case 3) as it represents the correct motion of the contact line observed during experiments. However, in the absence of suitable experimental data, a static contact angle value may be used (Case 1), but care must be taken to choose the value of static contact angle. It has been shown that the advancing contact angle has more influence on the bubble growth than the receding contact angle. Thus, choosing a mean value of the advancing and receding contact angles as the static contact angle will under predict the departure time. Also, with a static contact angle the bubble base variation will be smooth with no slip/stick behavior. On the other hand, if constant but different values of advancing and receding contact angles are used at the bubble base for calculations (Case 2) then it will over predict the departure time. It will also induce pronounced slip/stick behavior of the bubble base. However, as mentioned earlier the model of dynamic contact angle used at the bubble base will have little effect on the vapor volume growth rate.

6. Conclusions

Numerical simulation is carried out of single nucleating vapor bubble on a heated wall with different contact angle models at the bubble base. The following conclusions may be drawn from the above study:

1. Dynamic contact angle model based on the sign of the contact line velocity causes the bubble base to exhibit a stick/slip pattern during bubble growth whereas the base exhibits a smooth behavior when the static contact angle model is used.
2. Calculations based on experimental data show that there is little effect on the vapor volume growth rate whether a static or dynamic contact angle model is used.
3. The vapor volume growth rate is found to primarily increase with increase in the advancing contact angle.
4. Decrease in surface wettability results in a bubble with larger departure diameter which is more effective in disturbing the thermal boundary layer around it and increases the wall heat transfer, which is consistent with experimental observations.

Acknowledgements

The work was conducted in the Thermal Analysis and Microfluidics Laboratory at RIT. The support extended by the Mechanical Engineering Department and Gleason Chair Endowment is gratefully acknowledged.

References

[1] A. Mukherjee, Numerical and experimental study of lateral merger of vapor bubbles formed on a horizontal surface during nucleate pool, boiling, Ph.D. Thesis, University of California, Los Angeles, CA, 2003.
[2] R.-D. Schulze, W. Possart, H. Kamusewitz, C. Bischof, Young's equilibrium contact angle on rough solid surfaces. Part I. An empirical determination, J. Adhes. Sci. Technol. 3 (1) (1989) 39–48.
[3] M. Shoji, X.Y. Zhang, Study of contact angle hysteresis (in relation to boiling surface wettability), JSME Int. J., Series B 37 (3) (1994) 560–567.
[4] S. Brandon, A. Marmur, Simulation of contact angle hysteresis on chemically heterogeneous surfaces, J. Colloid Interface Sci. 183 (1996) 351–355.
[5] S.G. Kandlikar, M.E. Steinke, Contact angles and interface behavior during rapid evaporation of liquid on a heated surface, Int. J. Heat Mass Transfer 45 (2002) 3771–3780.
[6] C.N.C. Lam, R. Wu, D. Li, M.L. Hair, A.W. Neumann, Study of the advancing and receding contact angles: liquid sorption as a cause of contact angle hysteresis, Adv. Colloid Interface Sci. 96 (2002) 169–191.
[7] N. Ramanujapu, V.K. Dhir, Dynamics of contact angle during growth and detachment of a vapor bubble at a single nucleation site, in: Proceedings of the 5th ASME/JSME Joint Thermal Engineering Conference, San Diego, CA, 1999, AJTE99/6277.
[8] V.D. Sobolev, N.V. Churaev, M.G. Velarde, Z.M. Zorin, Surface tension and dynamic contact angle of water in thin quartz capillaries, J. Colloid Interface Sci. 222 (2000) 51–54.
[9] H.J. Barraza, S. Kunapuli, E.A. O'Rear, Advancing contact angles of Newtonian fluids during "high" velocity, transient, capillary-driven flow in a parallel plate geometry, J. Phys. Chem. B 106 (2002) 4979–4987.
[10] S.G. Kandlikar, W.K. Kuan, A. Mukherjee, Experimental study of heat transfer in an evaporating meniscus on a moving heated surface, J. Heat Transfer 127 (2005) 244–252.
[11] S.G. Kandlikar, B.J. Stumm, A control volume approach for investigating forces on a departing bubbles under subcooled flow boiling, J. Heat Transfer 117 (1995) 990–997.
[12] G. Son, V.K. Dhir, N. Ramanujapu, Dynamics and heat transfer associated with a single bubble during nucleate boiling on a horizontal surface, J. Heat Transfer 121 (1999) 623–631.
[13] S.G. Kandlikar, A theoretical model to predict pool boiling CHF incorporating effects of contact angle and orientation, J. Heat Transfer 123 (2001) 1071–1079.
[14] H.S. Abarajith, V.K. Dhir, A numerical study of the effect of contact angle on the dynamics of a single bubble during pool boiling, in: Proceedings of the ASME IMECE, New Orleans, LA, 2002, IMECE2002-33876.
[15] J. Fukai, Y. Shiiba, T. Yamamoto, O. Miyatake, D. Poulikakos, C.M. Megaridis, Z. Zhao, Wetting effects on the spreading of a liquid droplet colliding with a flat surface: experiment and modeling, Phys. Fluids 7 (2) (1995) 236–247.
[16] M. Bussman, J. Mostaghimi, S. Chandra, On a three-dimensional volume tracking model of droplet impact, Phys. Fluids 11 (6) (1999) 1406–1417.
[17] G. Son, N. Hur, A level set formulation for incompressible two-phase flows on nonorthogonal grids, Numer. Heat Transfer, Part B 48 (2005) 303–316.
[18] A. Mukherjee, V.K. Dhir, Study of lateral merger of vapor bubbles during nucleate pool boiling, J. Heat Transfer 126 (2004) 1023–1039.
[19] S.V. Patankar, Numerical Heat Transfer and Fluid Flow, Hemisphere Publishing Company, Washington DC, 1980.
[20] J.P. Van Doormaal, G.D. Raithby, Enhancements of the SIMPLE method for predicting incompressible fluid flows, Numer. Heat Transfer 7 (1984) 147–163.
[21] S.V. Patankar, A calculation procedure for two-dimensional elliptic situations, Numer. Heat Transfer 4 (1981) 409–425.
[22] M. Sussman, P. Smereka, S. Osher, A level set approach for computing solutions to incompressible two-phase flow, J. Comput. Phys. 114 (1994) 146–159.
[23] R.P. Fedkiw, T. Aslam, B. Merriman, S. Osher, A non-oscillatory Eulerian approach to interfaces in multimaterial flows (the ghost fluid

method), CAM Report 98-17, Department of Mathematics, UCLA, Los Angeles, CA, 1998.

[24] E.B. Dussan V, On the spreading of liquids on solid surfaces: static and dynamic contact lines, Annu. Rev. Fluid Mech. 11 (1979) 371–400.

[25] S.P. Liaw, V.K. Dhir, Void fraction measurements during saturated pool boiling of water on partially wetted vertical surfaces, J. Heat Transfer 111 (1989) 731–738.